Research Letter

How to Cite: *J. Inorg. Mater.*, 2026, **41(6):** 831
DOI: 10.15541/jim20250400

Highly Efficient EMI Shielding *via* 3D-printed CNT/SiC-SiO_2 Architectures

WANG Mengmeng[1,2,3], TIAN Li[2,3], ZHANG Junmin[1], LI Qinggang[1], YANG Jinshan[2,3], DONG Shaoming[2,3,4]

(1. Suzhou National Laboratory, Suzhou 215123, China; 2. State Key Laboratory of High Performance Ceramics, Shanghai Institute of Ceramics, Chinese Academy of Sciences, Shanghai 200050, China; 3. Structural Ceramics and Composites Engineering Research Center, Shanghai Institute of Ceramics, Chinese Academy of Sciences, Shanghai 200050, China; 4. Center of Materials Science and Optoelectronics Engineering, University of Chinese Academy of Sciences, Beijing 100049, China)

Abstract: The development of lightweight, mechanically robust, and high-performance electromagnetic interference (EMI) shielding materials is critical for next-generation electronic and communication systems. In this study, we report the design and fabrication of a 3D-printed carbon nanotube/polydimethylsiloxane (CNT/PDMS) composite with tunable composition and hierarchical architecture. The resulting composite exhibits exceptional mechanical resilience, supporting loads up to 250 times its own weight and recovering fully after experiencing 40% strain. During pyrolysis in an inert atmosphere, the PDMS matrix decomposes and transforms into a SiC-SiO_2 ceramic phase that encapsulates the CNT network, thereby forming a hierarchically porous, multi-phase architecture. Notably, the CNT/SiC-SiO_2 composite demonstrates outstanding EMI shielding effectiveness (SE) of 62.0 dB in the X-band (8–12 GHz), primarily attributed to absorption (SE_A=59.91 dB). This elevated absorption capability arises from synergistic effects including improved impedance matching, conduction loss, interfacial/dipole polarization, and multiple internal reflections within the hierarchically porous, multi-interface architecture. The "absorption-reflection-reabsorption" mechanism enables near-complete attenuation of incident electromagnetic waves. This work presents a scalable, 3D-printing-enabled strategy for fabricating multifunctional carbon-ceramic composites with superior EMI shielding performance, which can meet the requirement of aerospace, wearable electronics, and military applications.

Key words: electromagnetic interference (EMI); 3D printing; porous CNT/SiC-SiO_2 ceramic; EMI shielding absorption mechanism

The rapid advancement of electronic devices and telecommunications, particularly with the advance of the 5G era, has led to an exponential increase in electromagnetic pollution, underscoring the importance of effective electromagnetic interference (EMI) shielding in both civilian and military applications[1-3]. The reliable operation of sensitive electronics in consumer, industrial, and defense systems critically depends on high-performance EMI shielding materials[4]. Conventionally metallic shields, although highly conductive, primarily operate through a reflective shielding mechanism, which not only limits their effectiveness but also contributes to secondary electromagnetic pollution[5-7]. Additionally, their high density, susceptibility to corrosion, and limited processability pose significant challenges for modern lightweight and flexible electronic systems[8-10]. These limitations have spurred intense interest in developing lightweight, flexible, and absorption-dominant EMI shielding materials that offer superior performance with minimal environmental impact[11].

Carbon-based nanomaterials, especially carbon nanotubes (CNTs), have emerged as promising candidates for

Received date: 2025-10-13; **Revised date:** 2025-11-17; **Published online:** 2025-11-27
Foundation item: National Natural Science Foundation of China (52222202, 52502107); Shanghai Pilot Program for Basic Research–Chinese Academy of Science, Shanghai Branch (JCYJ-SHFY-2021-001)
Biography: WANG Mengmeng (1997–), female, PhD. E-mail: wangmm@szlab.ac.cn
王萌萌(1997−), 女, 博士. E-mail: wangmm@szlab.ac.cn
Corresponding author: YANG Jinshan, professor. E-mail: jyang@mail.sic.ac.cn; DONG Shaoming, professor. E-mail: smdong@mail.sic.ac.cn
杨金山, 研究员. E-mail: jyang@mail.sic.ac.cn; 董绍明, 研究员. E-mail: smdong@mail.sic.ac.cn

next-generation EMI shielding due to their exceptional electrical conductivity, large specific surface area, low density, and tunable dielectric properties[12-14]. Conventional fabrication methods of CNT-based composites often limit the geometric complexity and structural design freedom, thereby restricting their application in advanced systems that require tailored architectures[15-17].

Three-dimensional (3D) direct ink writing (DIW) has recently emerged as a powerful additive manufacturing strategy, enabling the precise fabrication of complex, multiscale architectures[18-21]. For CNT-based systems, this process requires not only a stable colloidal dispersion but also a matrix that maintains structural integrity during printing and subsequent processing. Polydimethylsiloxane (PDMS) is an ideal candidate due to its excellent flexibility, thermal stability, and compatibility with high-temperature treatments[22]. Notably, PDMS can serve a dual function: as a printable elastomeric matrix at room temperature and as a precursor for silicon carbide (SiC) and silicon dioxide (SiO_2) ceramics upon pyrolysis[23]. This capability enables the transformation of 3D-printed CNT/SiC-SiO_2 preforms into robust, porous carbon-ceramic hybrid scaffolds with enhanced mechanical and functional properties.

In this work, we present a high-performance 3D-printed CNT/PDMS composite ink and its conversion into a CNT/SiC-SiO_2 ceramic architecture through controlled pyrolysis to achieve a total shielding effectiveness (SE) of 62.0 dB, with the shielding contribution derived from absorption. This absorption-dominant behavior arises from improved impedance matching and the synergistic interplay between conductive CNTs and dielectric ceramic phases within the engineered 3D architecture. Our findings demonstrate a scalable and versatile approach to designing multifunctional, structurally robust EMI shielding materials by integrating 3D printing with polymer-derived ceramic technology.

1 Experimental

1.1 Materials and methods

Multi-walled carbon nanotubes (MWCNTs) used in this study were purchased from Adamas (China) and exhibited a length ranging from 30 to 50 μm. Absolute ethanol (≥95%) was used as the solvent for slurry preparation. Polydimethylsiloxane (PDMS, CAS 9016-00-6), a two-part liquid silicone consisting of a base and a curing agent, was utilized as the binder system and dispersing agent to enable structural integrity of the printed scaffold after curing.

A homogeneous slurry was prepared by dispersing the MWCNTs in absolute ethanol through ultrasonication (150 W, 2 h), as illustrated in Fig. 1(a). Subsequently, the PDMS base and curing agent were added to the well-dispersed CNT suspension at a predetermined weight ratio (14.1%, 14.5%, and 14.9%) and mixed thoroughly using mechanical stirring and further ultrasonication to ensure uniform incorporation while avoiding excessive bubbles. The resulting viscous ink was loaded into a syringe and printed into a 3D porous scaffold using a DIW 3D printer (3D Bioprinter V2.0, Hangzhou Jienuofei Biotechnology) equipped with a temperature-controlled stage. The moving speed of the printer nozzle was set between 1 and 30 mm/s, with an air pressure range of 0–0.6 MPa. After printing, the green body

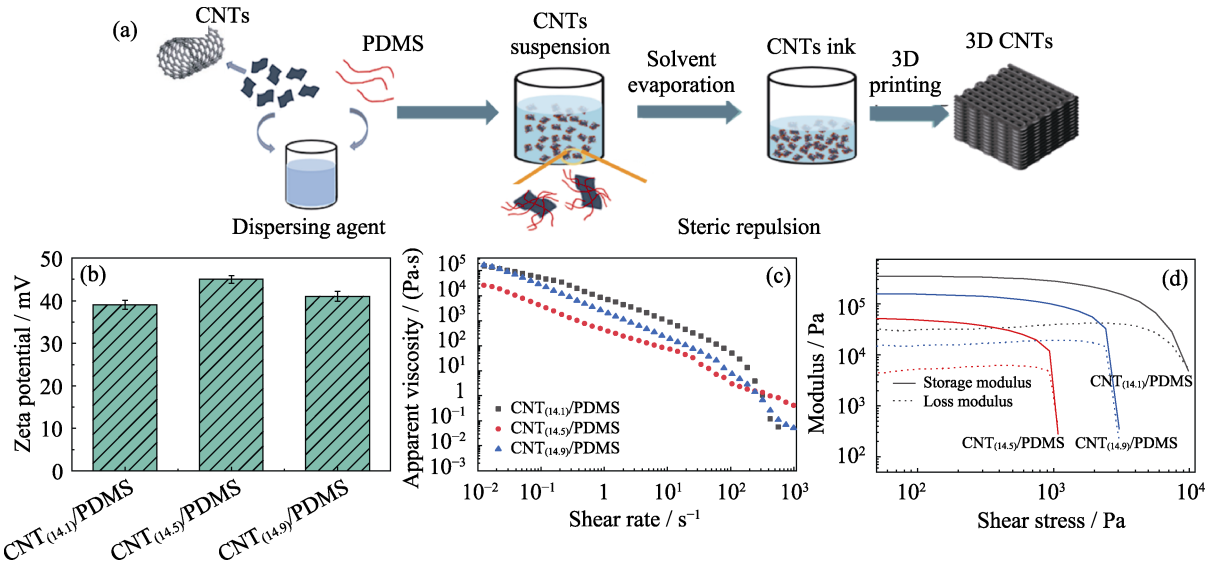

Fig. 1 (a) Schematic diagram of the preparation process; (b) Zeta potential, (c) apparent viscosity, (d) storage modulus and loss modulus of CNT/PDMS inks

underwent curing at 120 ℃ for 1 h to crosslink the PDMS binder, yielding a mechanically robust 3D CNT preform. The as-fabricated 3D CNT preform was subjected to pyrolysis in tube furnace under a flow of high-purity argon gas. The pyrolysis process was conducted at 1100 ℃ for 1 h, with a heating rate of 5 ℃/min from room temperature to 500 ℃, followed by a rate of 10 ℃/min from 500 to 1100 ℃. The as-prepared three samples are named as $CNT_{(14.1)}$/SiC-SiO_2, $CNT_{(14.5)}$/SiC-SiO_2, and $CNT_{(14.9)}$/SiC-SiO_2, where the numerical values correspond to the initial CNT mass fraction in the composite ink as shown in Table 1.

1.2 Characterization

The colloidal stability of MWCNTs suspension was evaluated by zeta potential measurement using a ZetaPlus analyzer (Brookhaven Instruments Corporation, USA). The rheological behavior of 3D printing ink was characterized using a rotational rheometer equipped with a parallel-plate geometry. The surface and cross-sectional morphology of the CNT/SiC-SiO_2 composites were examined using a field-emission scanning electron microscope (SEM, FEI Inspect F50, USA) operated at an accelerating voltage of 10 kV. Prior to SEM observation, samples were sputter-coated with a thin layer of gold to minimize charging effects. High-resolution nanoscale imaging and structural analysis were conducted using a field-emission transmission electron microscope (TEM, Hitachi JEM-2100F, Japan) at 200 kV. The surface chemical composition and bonding states were analyzed by X-ray photoelectron spectroscopy (XPS, Thermo Scientific K-Alpha 250Xi, USA). High-resolution scans of C1s and Si2p core levels were deconvoluted to determine the chemical environments and oxidation states of the elements present. The SE was tested in the frequency range of 8–12 GHz (X-band), and the *S* parameters (S_{11} and S_{22}) of the films were obtained using a Rohde & Schwarz ZVB20 vector network analyzer (VNA) by the waveguide transmission reflection method[24]. According to Schelkunoff's theory, the EMI SE can be evaluated based on the following formulas:

$$SE_T=SE_R+SE_A+SE_{MR} \quad (1)$$

$$A+R+T=1 \quad (2)$$

Table 1 Composition ratio of CNT/PDMS in the composite ink

Sample	CNT/g	Ethanol/g	PDMS base agent/g	PDMS curing agent/g	CNT/% (in mass)
$CNT_{(14.1)}$/PDMS	1	0.2	5	0.5	14.1
$CNT_{(14.5)}$/PDMS	1	0.4	5	0.5	14.5
$CNT_{(14.9)}$/PDMS	1	0.6	5	0.5	14.9

$$SE_R=-10\lg(1-R)=-10\lg(1-S_{11}^2) \quad (3)$$

$$SE_A=-10\lg[T/(1-R)]=-10\lg[S_{21}^2/(1-S_{11}^2)] \quad (4)$$

where SE_T is the total EMI SE, SE_R stands for the reflection efficiency, SE_A and SE_{MR} represent the absorption and multiple reflection efficiency, respectively. Moreover, *T*, *A* and *R* represent the power coefficients of electromagnetic transmission, wave absorption, and reflection, respectively.

2 Results and discussion

2.1 Mechanics analysis of CNT/PDMS composite

To quantitatively evaluate the colloidal stability of the CNT suspension, zeta potential measurements were performed on three samples of the dispersion, as depicted in Fig. 1(b). The zeta potential reflects the effective surface charge of dispersed particles and serves as a key indicator of electrostatic stabilization in colloidal systems. Generally, a higher absolute zeta potential value (typically>15 mV) indicates strong interparticle repulsion in ethanol, which inhibits agglomeration and promotes long-term dispersion stability[25]. The measured zeta potential values of $CNT_{(14.5)}$/PDMS exhibit absolute magnitudes exceeding 40 mV across repeated measurements. This finding confirms that the CNT, dispersant, and ethanol system forms a highly stable colloidal dispersion, where the stabilizing interactions dominate over van der Waals-driven aggregation forces. As shown in Fig. 1(c), the viscosity of the CNT/PDMS composite ink exhibits a strong dependence on shear rate, significantly decreasing as the shear rate increases. This characteristic is essential for direct ink writing during extrusion through the nozzle. The high shear rates of 50 s^{-1} at syringe needle can reduce the ink's viscosity to facilitate smooth, continuous flow. Under these conditions, the measured viscosity ranges from 100 to 500 Pa/s, which falls within the optimal window for extrusion-based printing of highly filled inks, ensuring processability without clogging or inconsistent filament deposition. As illustrated in Fig. 1(d), oscillatory rheological measurements reveal that the storage modulus (*G*′, representing elastic response) dominates over the loss modulus (*G*″, representing viscous response) at low shear stresses, thereby indicating a gel-like, solid-dominated network structure of CNT/PDMS composite ink. At a shear stress of 50 Pa, the storage modulus reaches values between 10^4 and 10^5 Pa, reflecting a robust internal network capable of maintaining shape fidelity and supporting multi-layered structures. Furthermore, the crossover points of *G*′ and *G*″ of three samples were determined in the shear stress range of 10^3–10^4 Pa. This high yield stress indicates that the ink remains mechanically stable under its own weight and external

disturbances during printing, only flowing when sufficient stress is applied during extrusion[26-28]. The strong shear-thinning behavior, combined with high yield stress and rapid elastic recovery, endows the CNT/PDMS ink with excellent printability and shape retention.

To evaluate the structural integrity and mechanical robustness of the 3D-printed CNT/PDMS composite, a series of mechanical tests were performed on a sample containing 14.5% CNTs. As illustrated in Fig. 2(a), a light weight $CNT_{(14.5)}$/PDMS specimen (0.4 g) successfully supported a load equivalent to 250 times its own mass without any visible deformation. This remarkable load-bearing capacity demonstrates the excellent mechanical stability of the printed architecture, which arises from the synergistic combination of the percolating CNT network and the reinforced PDMS matrix that effectively transfers and distributes applied stress. Further insight into the elastic behavior of the composite was gained through manual compression experiments, as depicted in Fig. 2(b). When compressed along the thickness direction by finger pressure and subsequently released, the sample fully recovered its original shape, indicating a high degree of elasticity. Notably, even under more severe deformation up to approximately 50% strain applied along the diagonal of the sample base, the structure exhibited complete shape recovery upon unloading.

To assess the mechanical response and energy dissipation characteristics, cyclic tensile loading-unloading tests were performed on miniaturized specimens (2 mm×2 mm) using a universal testing machine. The stress- strain curves under 10%, 20%, 30%, and 40% strain are presented in Fig. 2(c). At lower strain levels (0–10%), the loading and unloading curves closely overlap, exhibiting negligible hysteresis, which indicates highly reversible deformation with minimal internal friction or structural rearrangement. As the strain increases to 10% and 30%, a slight deviation between loading and unloading paths emerges, suggesting the onset of microstructural reorganization, such as CNT network slippage or localized PDMS relaxation. However, despite the presence of minor hysteresis, no significant residual strain is observed following full unloading, thereby confirming the excellent elastic recovery of the composite even under large deformations. The absence of permanent deformation up to 40% strain demonstrates the resilience of the 3D-printed architecture and the effectiveness of the PDMS in maintaining structural cohesion. The outstanding mechanical stability and elasticity of the $CNT_{(14.5)}$/PDMS preform are attributed to the uniform dispersion of CNTs and the reinforcing properties of PDMS, which provides both toughness and recovery capability.

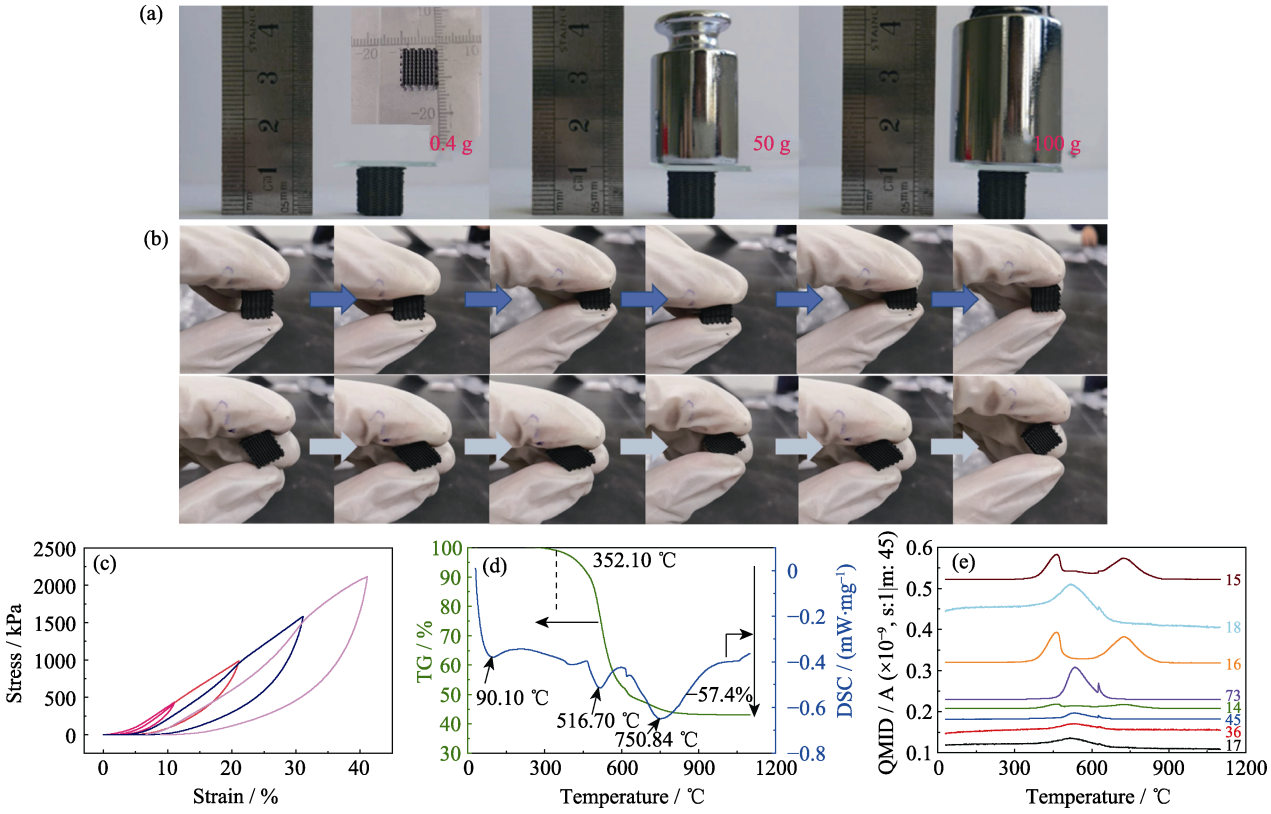

Fig. 2 (a) Mechanical compressive test diagram and (b) compress-release process in the direction of height and diagonal of bottom for $CNT_{(14.5)}$/PDMS; (c) Compressive stress-strain curves under 10%–40% strain; (d) Thermal gravimetric analysis and differential scanning calorimetry curve; (e) Mass spectra of $CNT_{(14.5)}$/PDMS

2.2 Morphology analysis of CNT/SiC-SiO_2 composite

To elucidate the thermal degradation mechanism and compositional changes, simultaneous thermogravimetric analysis (TGA) and differential scanning calorimetry (DSC) were performed under an inert atmosphere from room temperature to 1100 ℃, as shown in Fig. 2(d). The DSC curve reveals an initial endothermic peak at 90.10 ℃, corresponding to the evaporation of physically adsorbed moisture and residual ethanol solvent trapped within the porous network. This peak is accompanied by a minor mass loss observable in the TGA curve, consistent with the removal of volatile species. A more significant mass reduction occurs between 350 and 800 ℃, during which the TGA profile shows a sharp decline, accounting for the majority of the total weight loss. Concurrently, two prominent endothermic peaks are observed in the DSC signal at 516.70 and 750.84 ℃, attributed to the thermal decomposition of the PDMS matrix, residual dispersant, and associated organic components. At 1100 ℃, the cumulative mass loss reaches 57.4%, corresponding to the loss of organic phase, including PDMS, dispersant, and solvent. However, the measured residual mass exceeds the expected carbon content from CNTs alone, suggesting the formation of additional carbonaceous and silicon-containing residues during pyrolysis. This discrepancy is further supported by evolved gas analysis *via* mass spectrometry, as shown in Fig. 2(e), confirming the cleavage of organic functional groups from the PDMS backbone.

As illustrated in Fig. 3, the progressive thermal treatment leads to the scission of Si–C and C–H bonds alongside the elimination of methyl ($–CH_3$) groups from the PDMS structure. This process results in the gradual removal of organic side chains while concomitantly facilitating the formation of inorganic Si–O–Si and Si–C networks. The increasing intensity of Si–O and C–Si bonding components in the Si2p and C1s spectra indicates a transition from an organosilicon polymer to a partially ceramic, crosslinked amorphous network rich in SiC and SiO_2-like phases.

Morphological evolution before and after pyrolysis was examined *via* SEM. Prior to heat treatment, the as-printed $CNT_{(14.5)}$/PDMS scaffold exhibits a dense, entangled morphology with non-uniform pore distribution, as shown in Fig. 4(a), where the PDMS matrix encapsulates CNT bundles. After pyrolysis, a well-defined, interconnected porous architecture emerges, characterized by a honeycomb-like 3D network with enlarged interstitial spaces between CNT bundles, as depicted in Fig. 4(b). This transformation arises from the volatilization of organic components, resulting in a thermally stable, open-framework structure composed primarily of CNTs and pyrolytic carbon/silicon oxycarbide residues. Importantly, the adjacent CNT bundles remain in close contact, preserving the mechanical integrity of the scaffold despite significant mass loss. As illustrated in Figs. 4(c-f), the TEM images reveal a remarkable encapsulation of CNT bundles by finely dispersed SiC and SiO_2 phases. This intimate contact between the ceramic matrix and the carbon nanotubes is crucial for enhancing the overall mechanical properties of the composite. TEM observations indicate that both SiC and SiO_2 form continuous layers around the CNTs, effectively wrapping them in a uniform coating.

2.3 Electromagnetic shielding performance of CNT/SiC-SiO_2 composites

To evaluate the EMI SE of the 3D-printed CNT/SiC-SiO_2 composites, measurements were conducted across the X-band frequency range (8–12 GHz), as shown in Fig. 5(a). The SE_T was determined from the sum of SE_A, SE_R and SE_{MR} components. As illustrated in Fig. 5(b),

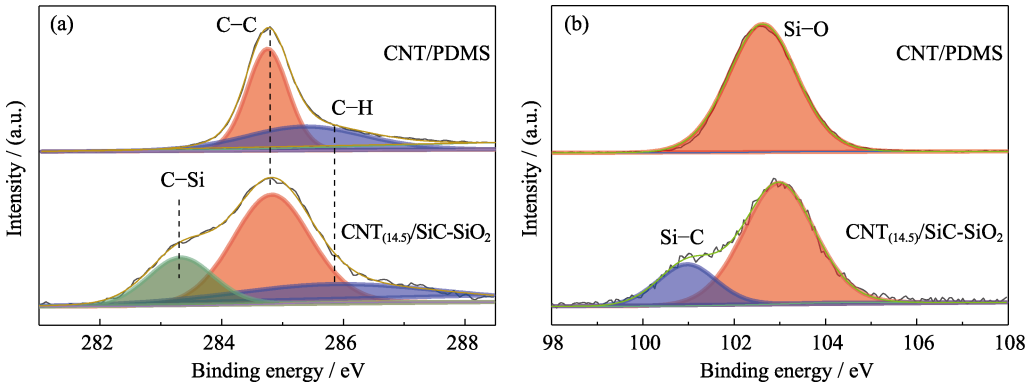

Fig. 3　XPS spectra of (a) C1s and (b) Si2p core level for CNT/PDMS before pyrolysis and $CNT_{(14.5)}$/SiC-SiO_2 after pyrolysis

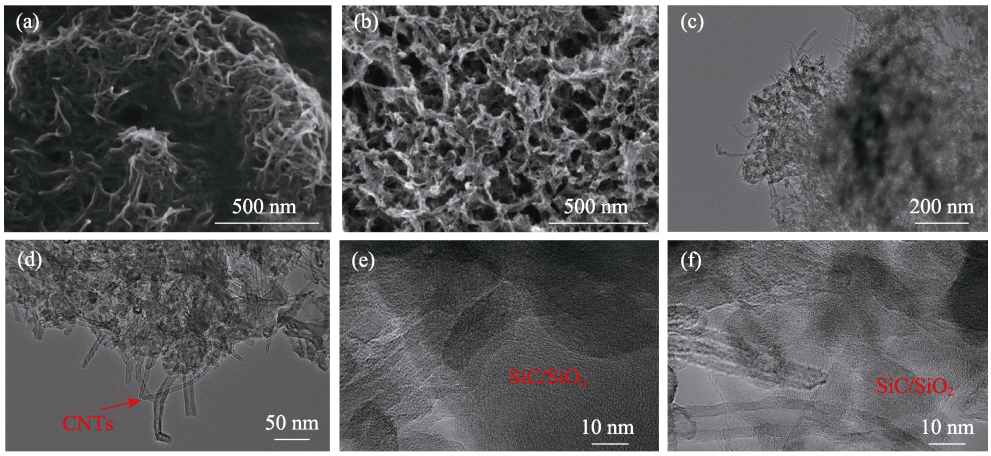

Fig. 4 (a, b) SEM images of 3D-printed (a) $CNT_{(14.5)}$/PDMS and (b) $CNT_{(14.5)}$/SiC-SiO_2; (c-f) TEM images of 3D-printed $CNT_{(14.5)}$/SiC-SiO_2

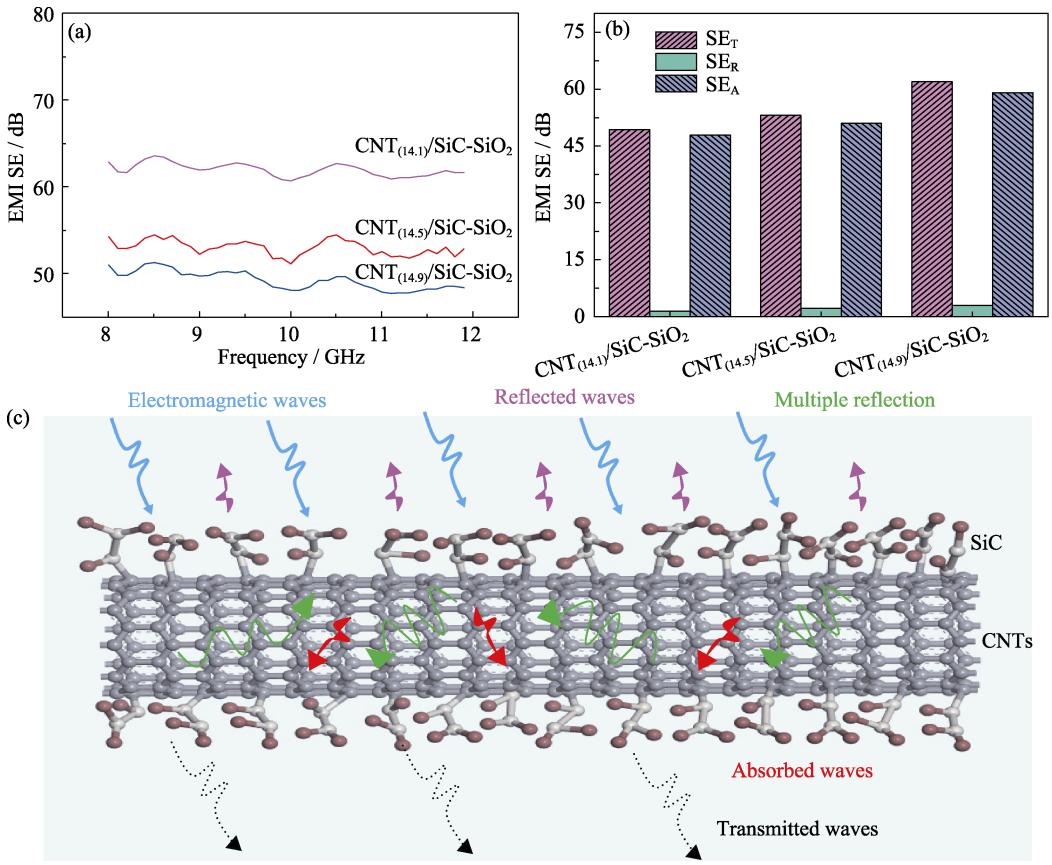

Fig. 5 (a) EMI shielding performance of CNT/SiC-SiO_2; (b) Average SE_T, SE_R, and SE_A, and (c) schematic illustration of the EMI shielding mechanism for CNT/SiC-SiO_2

the average SE_T of the composite with 14.1% (in mass) CNT loading reaches 49.3 dB, which sufficiently meets the requirements for commercial application (≥30 dB). However, fine-tuning the CNT content to 14.5% (in mass) results in a significant increase in SE_T, achieving 62.0 dB and fulfilling the requirements of military-grade shielding applications (≥60 dB). This level of shielding performance has surpassed most reported materials, such as 3D graphene-CNT-SiC (29 dB)[29], SiCNWs@CNTs (47.99 dB)[30], SiBCN-CNT (40 dB)[31], SiC_{nws}/CNFs/SiC (57.2 dB)[32], RGO/MWCNTs (57.36 dB)[33], *etc*. Notably, the SE_A component increases from 47.9 dB for $CNT_{(14.1)}$/SiC-SiO_2 to 59.9 dB for $CNT_{(14.5)}$/SiC-SiO_2, indicating that the enhancement in overall shielding is predominantly attributed to absorption rather than reflection. This characteristic is highly desirable, as absorptive shielding minimizes secondary electromagnetic pollution, thereby rendering the material more

suitable for practical applications in sensitive electronic environments. The superior absorption-dominant EMI shielding behavior of the $CNT_{(14.5)}$/SiC-SiO_2 composite can be attributed to two key factors: improved impedance matching and efficient electromagnetic wave attenuation through multiple loss mechanisms in Fig. 5(c).

Firstly, the surface-modified structure with a coating of SiC/SiO_2 derived from PDMS pyrolysis reduces the impedance mismatch between free space and the composite surface. The SiC/SiO_2 heterostructure enables impedance matching by optimizing the balance between conductivity and dielectric properties[34]. This enhancement allows incident electromagnetic waves to penetrate more readily into the interior of the material, rather than being immediately reflected, thereby increasing the opportunity for internal absorption. Secondly, once within the material, the electromagnetic waves encounter a hierarchically porous, multi-phase architecture that promotes extensive energy dissipation *via* several concurrent mechanisms: conduction loss, interfacial and dipole polarization losses, and multiple internal reflections and scattering. The presence of semi-conductive SiC nanoparticles and conductive CNTs establishes conductive pathways throughout the matrix. Under alternating electromagnetic fields, these networks support microcurrents, leading to Joule heating and conversion of electromagnetic energy into thermal energy. Numerous heterogeneous interfaces, such as SiC/SiC, SiC/CNT, SiO_2/CNT, SiC/SiO_2, and CNT/CNT, are formed due to the nanoscale dispersion of ceramic phases within the carbon framework. The significant differences in electrical conductivity and dielectric constant across these interfaces induce interfacial polarization, while defects and functional groups contribute to dipole polarization under dynamic electromagnetic fields. The 3D-printed scaffold exhibits a well-defined, honeycomb-like porous morphology after thermal treatment, creating abundant internal surfaces and voids. These features act as scattering centers, prolonging the propagation path of electromagnetic waves through repeated reflection, refraction, and reabsorption. This “absorption-reflection-reabsorption” mechanism ensures progressive attenuation of wave intensity prior to any transmission occurring.

3 Conclusions

In conclusion, this study successfully developed a 3D-printed CNT/PDMS composite that served as a precursor for a structurally robust and functionally advanced CNT/SiC-SiO_2 ceramic scaffold. The CNT/PDMS composite preforms outstanding mechanical performance, including the ability to support loads 250 times their own mass and full elastic recovery after up to 40% tensile strain. Critically, the $CNT_{(14.5)}$/SiC-SiO_2 exhibits exceptional EMI shielding performance in the X-band (8–12 GHz), achieving a SE_T of 62.0 dB. The synergy between the conductive CNT framework, dielectric SiC/SiO_2 phases, and engineered 3D architecture enables a cascading “absorption-reflection-reabsorption” process that maximizes electromagnetic wave attenuation. This work demonstrates a novel, scalable approach to fabricate multifunctional 3D printing composites that simultaneously address the demands of mechanical durability, thermal stability, and high-efficiency EMI shielding applications.

References:

[1] WANG X X, CAO W Q, CAO M S, *et al*. Assembling nano-microarchitecture for electromagnetic absorbers and smart devices. *Advanced Materials*, 2020, **32(36):** 2002112.

[2] AKRAM S, ASHRAF M, JAVID A, *et al*. Recent advances in electromagnetic interference (EMI) shielding textiles: a comprehensive review. *Synthetic Metals*, 2023, **294:** 117305.

[3] ORASUGH J T, RAY S S. Functional and structural facts of effective electromagnetic interference shielding materials: a review. *ACS Omega*, 2023, **8(9):** 8134.

[4] HOU X, FENG X R, JIANG K, *et al*. Recent progress in smart electromagnetic interference shielding materials. *Journal of Materials Science & Technology*, 2024, **186:** 256.

[5] ISARI A A, GHAFFARHHAH A, HASHEMI S A, *et al*. Structural design for EMI shielding: from underlying mechanisms to common pitfalls. *Advanced Materials*, 2024, **36(24):** 2310683.

[6] WANG H, LI S, LIU M, *et al*. Review on shielding mechanism and structural design of electromagnetic interference shielding composites. *Macromolecular Materials and Engineering*, 2021, **306(6):** 2100032.

[7] ZHAO H, WANG J, HE M, *et al*. Electromagnetic interference shielding films: structure design and prospects. *Small Methods*, 2025, **9(5):** 2401324.

[8] YAO Y, JIN S, ZOU H, *et al*. Polymer-based lightweight materials for electromagnetic interference shielding: a review. *Journal of Materials Science*, 2021, **56(11):** 6549.

[9] WANG M, TIAN L, ZHANG Q, *et al*. Absorption-based electromagnetic interference shielding composites with sandwich structure by one-step electrodeposition method. *Carbon*, 2023, **202:** 414.

[10] WANG M, YOU X, LIAO C, *et al*. Ultrathin and flexible hybrid films decorated by copper nanoparticles with a sandwich-like structure for electromagnetic interference shielding. *Materials Chemistry Frontiers*, 2022, **6(16):** 2256.

[11] SATHISH K, RENGARAJ R, VENKATAKRISHNAN G R, *et al*. Polymeric materials for electromagnetic shielding-a review. *Materials Today: Proceedings*, 2021, **47:** 4925.

[12] XUE Z, CORDIER R, KNIGHT E, *et al*. Lightweight, flexible electromagnetic shielding composite films reinforced with recycled carbon fibers and carbon nanofillers. *Advanced Engineering Materials*, 2025, **27(22):** e202501907.

[13] CUI L, HAN X, WANG F, *et al*. A review on recent advances in carbon-based dielectric system for microwave absorption. *Journal of Materials Science*, 2021, **56(18):** 10782.

[14] AYANDA O S, MMUOEGBULAM A O, OKEZIE O, *et al*. Recent progress in carbon-based nanomaterials: critical review. *Journal of Nanoparticle Research*, 2024, **26(5):** 106.

[15] AL-SALEH M H. Influence of conductive network structure on the EMI shielding and electrical percolation of carbon nanotube/polymer nanocomposites. *Synthetic Metals*, 2015, **205:** 78.
[16] KUMAR S. Investigating effect of CNT agglomeration in CNT/polymer nanocomposites using multiscale finite element method. *Mechanics of Materials*, 2023, **183:** 104706.
[17] WANG M, YANG J, YOU X, *et al*. Nanoinfiltration behavior of carbon nanotube based nanocomposites with enhanced mechanical and electrical properties. *Journal of Materials Science & Technology*, 2021, **71:** 23.
[18] PANDAYA K S, SHINDALKAR S S, KANDASUBRAMANIAN B. Breakthrough to the pragmatic evolution of direct ink writing: progression, challenges, and future. *Progress in Additive Manufacturing*, 2023, **8(6):** 1303.
[19] ZHAO Y, ZHU J, HE W, *et al*. 3D printing of unsupported multi-scale and large-span ceramic *via* near-infrared assisted direct ink writing. *Nature Communications*, 2023, **14:** 2381.
[20] CIDONIO G, COSTANTINI M, PIERINI F, *et al*. 3D printing of biphasic inks: beyond single-scale architectural control. *Journal of Materials Chemistry C*, 2021, **9(37):** 12489.
[21] XU X, TAN Y H, DING J, *et al*. 3D printing of next-generation electrochemical energy storage devices: from multiscale to multi-material. *Energy & Environmental Materials*, 2022, **5(2):** 427.
[22] SHI Y, HU M, XING Y, *et al*. Temperature-dependent thermal and mechanical properties of flexible functional PDMS/paraffin composites. *Materials & Design*, 2020, **185:** 108219.
[23] REN Z, MUJIB S B, SINGH G. High-temperature properties and applications of Si-based polymer-derived ceramics: a review. *Materials*, 2021, **14(3):** 614.
[24] WANG M, TIAN L, YOU X, *et al*. Flexible, magnetic and sandwich-structural Fe_2O_3/CNT/Fe_2O_3 composite film with absorption-dominant EMI shielding performance. *Journal of Materials Science & Technology*, 2025, **227:** 122.
[25] ZHAO L, GAO L. Stability of multi-walled carbon nanotubes dispersion with copolymer in ethanol. *Colloids and Surfaces A: Physicochemical and Engineering Aspects*, 2003, **224:** 127.
[26] FU K, WANG Y, YAN C, *et al*. Graphene oxide-based electrode inks for 3D-printed lithium-ion batteries. *Advanced Materials*, 2016, **28(13):** 2587.
[27] COMPTON B G, LEWIS J A. 3D-printing of lightweight cellular composites. *Advanced Materials*, 2014, **26(34):** 5930.
[28] KIM J H, LEE S, WAJAHAT M, *et al*. Three-dimensional printing of highly conductive carbon nanotube microarchitectures with fluid ink. *ACS Nano*, 2016, **10(9):** 8879.
[29] FENG F, HAN Z, WEI B, *et al*. Increasing both the electromagnetic shielding and thermal conductive properties of three-dimensional graphene-CNT-SiC hybrid materials. *New Carbon Materials*, 2024, **39(6):** 1178.
[30] LIU H, ZHANG X, LI K, *et al*. Construction of core-shell structured SiC nanowires@carbon nanotubes hybrid conductive network for supercapacitors and electromagnetic interference shielding. *Carbon*, 2024, **228:** 119411.
[31] LIU Y, YANG F, GU H, *et al*. Flexible CNT-based composite films with amorphous SiBCN-inhibited ultrafine SiC grains for high-temperature electromagnetic shielding. *Ceramics International*, 2024, **50(21):** 41057.
[32] YANG Y, YOU X, OUYANG H, *et al*. Electromagnetic interference shielding properties of foamed SiCnws/SiC composites reinforced by *in-situ* grown carbon nanofibers. *Journal of Alloys and Compounds*, 2024, **1008:** 176641.
[33] XIA Y, ZHANG Z, LI K, *et al*. Lightweight and high-strength SiC/MWCNTs nanofibrous aerogel derived from RGO/MWCNTs aerogel for microwave absorption. *Chemical Engineering Journal*, 2024, **486:** 50417.
[34] YU S, GUO J, ZHANG G, *et al*. Improved broadband design of SiC/MWCNT absorbing materials through synergistic regulation of heterointerface structure and triple periodic minimal surface meta-structure. *Carbon*, 2024, **226:** 119181.

3D 打印制备 CNT/SiC-SiO_2 及其电磁屏蔽性能

王萌萌[1,2,3], 田 力[2,3], 张俊敏[1], 李庆刚[1], 杨金山[2,3], 董绍明[2,3,4]

(1. 苏州国家实验室, 苏州 215123; 2. 中国科学院 上海硅酸盐研究所, 关键陶瓷材料全国重点实验室, 上海 200050; 3. 中国科学院 上海硅酸盐研究所, 结构陶瓷与复合材料工程研究中心, 上海 200050; 4. 中国科学院大学 材料与光电研究中心, 北京 100049)

摘 要: 兼具轻质、优异力学性能和高电磁屏蔽效能的材料对下一代电子与通信系统的开发至关重要。本研究报道了一种通过 3D 打印设计和制备组分可控且具有多级结构的碳纳米管/聚二甲硅氧烷(CNT/PDMS)复合材料。该材料表现出卓越的机械性能, 可承受高达自身质量 250 倍的载荷, 并在 40%应变后完全恢复至原状。在惰性气氛下的热解过程中, PDMS 基体分解并转化为 SiC-SiO_2 陶瓷相, 包裹 CNT 网络, 形成具有多级多孔和多相结构的复合材料。CNT/SiC-SiO_2 复合材料在 X 波段(8~12 GHz)展现出高达 62 dB 的优异电磁屏蔽效能, 其中电磁吸收占主导(SE_A=59.91 dB)。这种高吸收能力源于多种协同效应, 包括优化阻抗匹配、导电损耗、界面/偶极极化以及在多级多孔、多界面结构内的多次反射。“吸收-反射-再吸收”机制实现了对入射电磁波近乎完全的衰减。本工作提出了一种基于 3D 打印的可扩展策略, 用于制备卓越电磁屏蔽性能的碳-陶瓷复合材料, 可满足航空航天、可穿戴电子器件和军事领域的应用需求。

关 键 词: 电磁干扰; 3D 打印; 多孔 CNT/SiC-SiO_2 陶瓷; 电磁干扰屏蔽吸收机制

中图分类号: TQ174 **文献标志码:** A **文章编号:** 1000-324X(2026)06-0831-08